22. COSMIC BACKGROUND RADIATION

Revised February 2001 by G.F. Smoot (University of California at Berkeley and LBNL) and D. Scott (University of British Columbia).

22.1. Introduction

The observed cosmic microwave background (CMB) radiation provides strong evidence for the hot big bang. The success of primordial nucleosynthesis calculations (see Sec. 19, "Big-bang nucleosynthesis") requires a cosmic background radiation (CBR) characterized by a temperature $kT \sim 1\,\mathrm{MeV}$ at a redshift of $z \simeq 10^9$. In their pioneering work, Gamow, Alpher, and Herman [1] realized this and predicted the existence of a faint residual relic, primordial radiation, with a present temperature of a few degrees. The observed CMB is interpreted as the current manifestation of the required CBR.

The CMB was serendipitously discovered by Penzias and Wilson [2] in 1965. Its spectrum is well characterized by a 2.73 K black-body (Planckian) spectrum over more than three decades in frequency (see Fig. 22.1). A non-interacting Planckian distribution of temperature T_i at redshift z_i transforms with the universal expansion to another Planckian distribution at redshift z_f with temperature $T_\mathrm{f}/(1+z_\mathrm{f}) = T_\mathrm{i}/(1+z_\mathrm{i})$. Hence the thermal spectrum, once established (*e.g.* at the nucleosynthesis epoch or earlier), is preserved by the expansion, in spite of the fact that photons decoupled from matter at early times. Atomic fine structure line observations along the lines of sight to distant quasars constrain the temperature at $z \approx 2$–3, giving direct support for the CMB being hotter at early times [3]. Because there are about 10^9 photons per nucleon, the transition from the ionized primordial plasma to neutral atoms at $z \sim 1000$ does not significantly alter the CBR spectrum [4]. CMB temperature variations observed at this epoch provide further support for the hot big bang, as well as for the presence of primordial density perturbations which grew into today's cosmological structure through gravitational instability.

22.2. The CMB frequency spectrum

The remarkable precision with which the CMB spectrum is fitted by a Planckian distribution provides limits on possible energy releases in the early Universe, at roughly the fractional level of 10^{-4} of the CBR energy, for redshifts $\lesssim 10^7$ (corresponding to epochs $\gtrsim 1\,\mathrm{year}$). The following three important classes of theoretical spectral distortions (see Fig. 22.2) generally correspond to energy releases at different epochs. The distortion results from the CBR photon interactions with a hot electron gas at temperature T_e.

22.2.1. ***Compton distortion***: Late energy release ($z \lesssim 10^5$). Compton scattering ($\gamma e \to \gamma' e'$) of the CBR photons by a hot electron gas creates spectral distortions by transferring energy from the electrons to the photons. Compton scattering cannot produce a Planckian spectrum for $y \lesssim 1$, where

$$y = \int_0^z \frac{kT_e(z') - kT_\gamma(z')}{m_e c^2}\, \sigma_T\, n_e(z')\, c\, \frac{dt}{dz'}\, dz' \,, \tag{22.1}$$

is the integral of the number of interactions, $\sigma_T\, n_e(z)\, c\, dt$, times the mean-fractional photon-energy change per collision [5]. For $T_e \gg T_\gamma$ y is also proportional to the integral

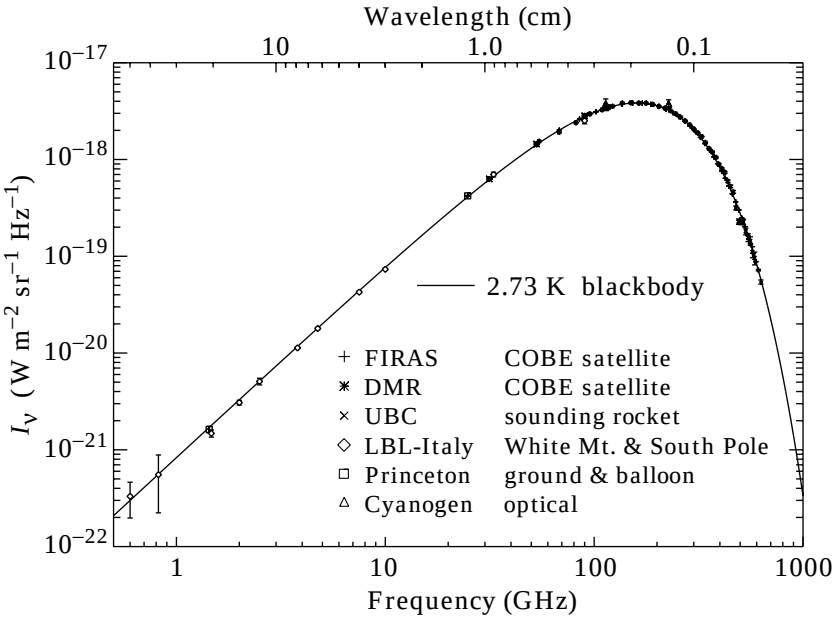

Figure 22.1: Precise measurements of the CMB spectrum. The line represents a 2.73 K blackbody, which describes the spectrum very well, especially around the peak of intensity. The spectrum is less well constrained at 10 cm and longer wavelengths. (References for this figure are at the end of this section under "CMB Spectrum References.")

of the electron pressure $n_e k T_e$ along the line of sight. For standard thermal histories $y < 1$ for epochs later than $z \simeq 10^5$.

The resulting CMB distortion is a temperature decrement

$$\Delta T_{\rm RJ} = -2y\, T_\gamma \tag{22.2}$$

in the Rayleigh-Jeans ($x \equiv h\nu/kT \ll 1$) portion of the spectrum, and a rise in temperature in the Wien ($x \gg 1$) region, *i.e.* photons are shifted from low to high frequencies. The magnitude of the distortion is related to the total energy transfer [5] ΔE by

$$\Delta E/E_{\rm CBR} = e^{4y} - 1 \simeq 4y\ . \tag{22.3}$$

A prime candidate for producing a Comptonized spectrum is a hot intergalactic medium. A hot ($T_e > 10^5$ K) medium in clusters of galaxies can and does produce a partially Comptonized spectrum as seen through the cluster, known as the Sunyaev-Zel'dovich effect [6]. Based upon X-ray data, the predicted large angular scale total combined effect of the hot intracluster medium should produce $y \sim 10^{-6}$ [7]. Detection of the S-Z effect through clusters demonstrates that the CMB is universal and can be used to estimate the Hubble constant, and counts of such clusters as a function of redshift hold the promise of constraining the equation of state of the Dark Energy.

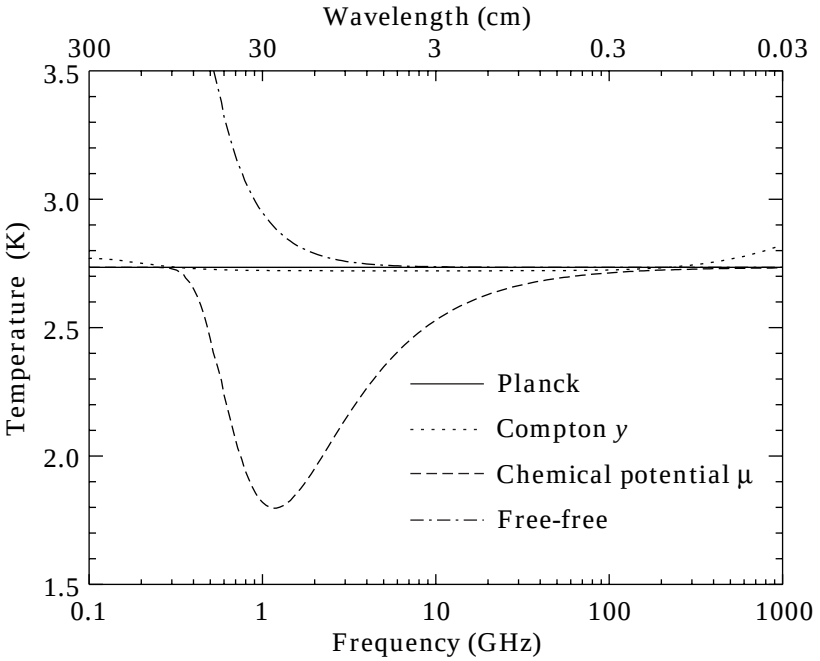

Figure 22.2: The shapes of expected, but so far unobserved, CMB distortions, resulting from energy-releasing processes at different epochs.

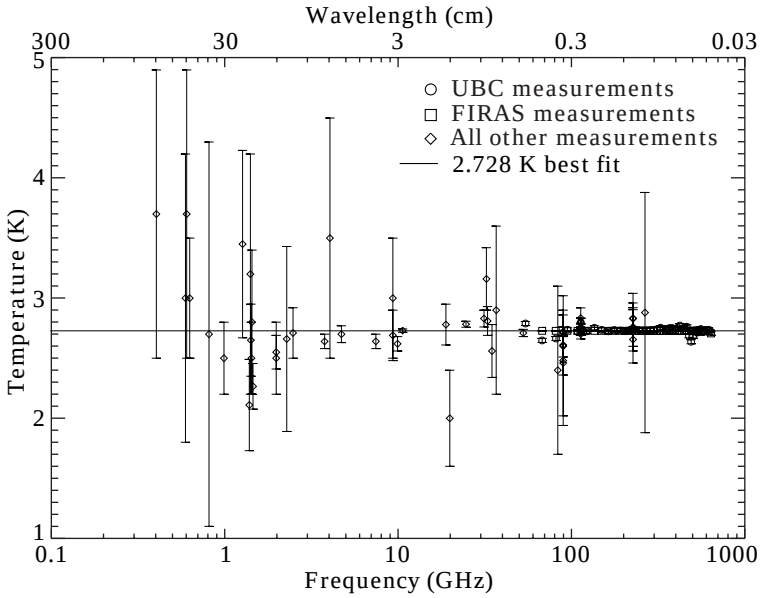

Figure 22.3: Observed thermodynamic temperature as a function of frequency.

22.2.2. ***Bose-Einstein or chemical potential distortion***: Early energy release ($z \sim 10^5$–10^7). After many Compton scatterings ($y \gg 1$), the photons and electrons will reach statistical (not thermodynamic) equilibrium, because Compton scattering conserves photon number. This equilibrium is described by the Bose-Einstein distribution with non-zero chemical potential:

$$n = \frac{1}{e^{x+\mu_0} - 1} \ , \tag{22.4}$$

where $x \equiv h\nu/kT$ and $\mu_0 \simeq 1.4\ \Delta E/E_{\rm CBR}$, with μ_0 being the dimensionless chemical potential that is required to conserve photon number. The collisions of electrons with nuclei in the plasma produce free-free (thermal bremsstrahlung) radiation: $eZ \to e'Z'\gamma$. Free-free emission thermalizes the spectrum to the plasma temperature at long (> centimeter) wavelengths.

The equilibrium Bose-Einstein distribution results from the oldest non-equilibrium processes ($10^5 < z < 10^7$), such as the decay of relic particles or primordial inhomogeneities. Note that free-free emission (thermal bremsstrahlung) and radiative-Compton scattering effectively erase any distortions [8] to a Planckian spectrum for epochs earlier than $z \sim 10^7$.

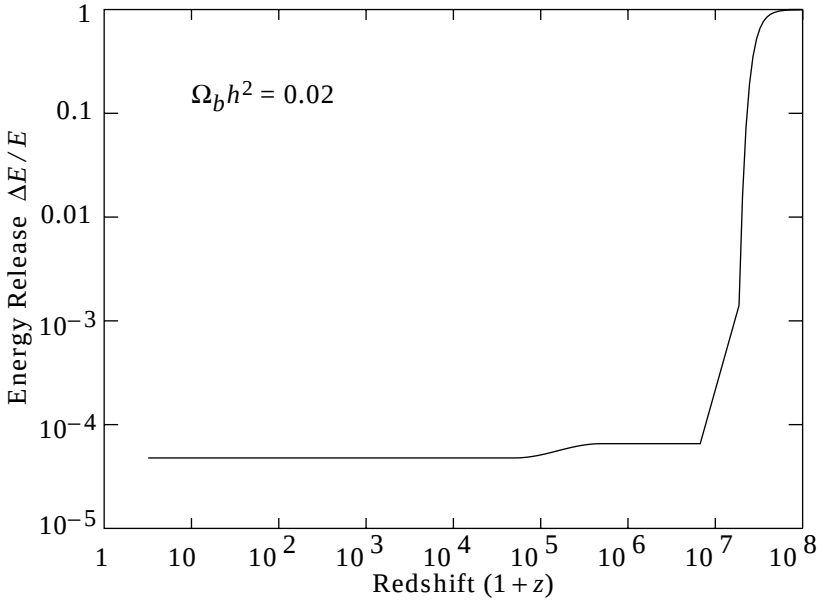

Figure 22.4: Upper limits (95% CL) on fractional energy ($\Delta E/E_{\rm CBR}$) releases from processes at different epochs as set by resulting lack of CMB spectral distortions. These can be translated into constraints on the mass, lifetime and photon branching ratio of unstable relic particles, with some additional dependence on cosmological parameters such as Ω_B [11]. This figure shows that the observed CMB spectrum is a relic from $z \sim 10^7$, $t \sim 1$ year.

22.2.3. ***Free-free distortion***: Very late energy release ($z \ll 10^3$). Free-free emission can create rather than erase spectral distortion in the late Universe, for recent reionization ($z < 10^3$) and from a warm intergalactic medium. The distortion arises because of the lack of Comptonization at recent epochs. The effect on the present-day CMB spectrum is described by

$$\Delta T_{\rm ff} = T_\gamma \, Y_{\rm ff}/x^2, \tag{22.5}$$

where T_γ is the undistorted photon temperature, $x \equiv h\nu/kT$ is the dimensionless frequency, and $Y_{\rm ff}/x^2$ is the optical depth to free-free emission:

$$Y_{\rm ff} = \int_0^z \frac{T_e(z') - T_\gamma(z')}{T_e(z')} \frac{8\pi e^6 h^2 n_e^2 \, g}{3 m_e (kT_\gamma)^3 \sqrt{6\pi \, m_e \, kT_e}} \frac{dt}{dz'} dz' \ . \tag{22.6}$$

Here h is Planck's constant, n_e is the electron density and g is the Gaunt factor [9].

22.2.4. ***Spectrum summary***: The CMB spectrum is consistent with a blackbody distribution over more than three decades of frequency around the peak. The best-fit to the COBE FIRAS data yields $T_\gamma = 2.725 \pm 0.002$ K (95% CL) [10]. The following table is a summary of all CMB spectrum measurements:

$$\begin{aligned}
&T_\gamma = 2.725 \pm 0.002 \text{ K} \quad (95\% \text{ CL}) \, ; \\
&n_\gamma = (2\zeta(3)/\pi^2) \, T_\gamma^3 \simeq 411 \, \text{cm}^{-3} \, ; \\
&\rho_\gamma = (\pi^2/15) \, T_\gamma^4 \simeq 4.64 \times 10^{-34} \, \text{g cm}^{-3} \simeq 0.260 \, \text{eV cm}^{-3} \, ; \\
&|y| < 1.2 \times 10^{-5} \qquad (95\% \text{ CL}) \, ; \\
&|\mu_0| < 9 \times 10^{-5} \qquad (95\% \text{ CL}) \, ; \\
&|Y_{\rm ff}| < 1.9 \times 10^{-5} \qquad (95\% \text{ CL}) \, .
\end{aligned}$$

These limits [12] correspond to constraints [12–14] on energetic processes $\Delta E/E_{\rm CBR} < 2 \times 10^{-4}$ occurring between redshifts 10^3 and 10^7 (see Fig. 22.4).

22.3. Deviations from isotropy

Penzias and Wilson reported that the CMB was isotropic and unpolarized at the 10% level. Current observations show that the CMB is unpolarized at the 10^{-5} level but has a dipole anisotropy at the 10^{-3} level, with smaller-scale anisotropies at the 10^{-5} level now measured over a wide range of angular scales.

It is customary to express the CMB temperature anisotropies on the sky in a spherical harmonic expansion,

$$\frac{\Delta T}{T}(\theta, \phi) = \sum_{\ell m} a_{\ell m} Y_{\ell m}(\theta, \phi) \ , \tag{22.7}$$

and to discuss the various multipole amplitudes. The power at a given angular scale θ, corresponding roughly to $\sim 1/\ell$, is $\ell \sum_m |a_{\ell m}|^2 / 4\pi$.

22.3.1. ***The dipole***: The largest anisotropy is in the $\ell = 1$ (dipole) first spherical harmonic, with amplitude at the level of $\Delta T/T = 1.23 \times 10^{-3}$. The dipole is interpreted as the result of the Doppler shift caused by the solar system motion relative to the nearly isotropic blackbody field, as confirmed by measurements of the velocity field of local galaxies [15]. The motion of the observer (receiver) with velocity $\beta = v/c$ relative to an isotropic Planckian radiation field of temperature T_0 produces a Doppler-shifted temperature

$$\begin{aligned} T(\theta) &= T_0(1-\beta^2)^{1/2}/(1-\beta\cos\theta) \\ &= T_0\,\left(1+\beta\cos\theta+(\beta^2/2)\cos 2\theta+O(\beta^3)\right)\ . \end{aligned} \tag{22.8}$$

The implied velocity [12,16] for the solar-system barycenter is $\beta = 0.001237 \pm 0.000002$ (68% CL) or $v = 371 \pm 0.5\,\mathrm{km\,s^{-1}}$, assuming a value $T_0 = T_\gamma$, towards $(\alpha, \delta) = (11.20^\mathrm{h} \pm 0.01^\mathrm{h}, -7.22^\circ \pm 0.08^\circ)$, or $(\ell, b) = (264.31^\circ \pm 0.17^\circ, 48.05^\circ \pm 0.10^\circ)$. Such a solar-system velocity implies a velocity for the Galaxy and the Local Group of galaxies relative to the CMB. The derived velocity is $v_\mathrm{LG} = 627 \pm 22\,\mathrm{km\,s^{-1}}$ toward $(\ell, b) = (276^\circ \pm 3^\circ, 30^\circ \pm 3^\circ)$, where most of the error comes from uncertainty in the velocity of the solar system relative to the Local Group.

The Doppler effect of this velocity and of the velocity of the Earth around the Sun, as well as any velocity of the receiver relative to the Earth, is normally removed for the purposes of CMB anisotropy study. The resulting high degree of CMB isotropy is the strongest evidence for the validity of the Robertson-Walker metric.

22.3.2. ***The quadrupole***: The rms quadrupole anisotropy amplitude is defined through $Q^2_\mathrm{rms}/T^2_\gamma = \sum_m |a_{2m}|^2/4\pi$. The current estimate of its value is $4\,\mu\mathrm{K} \le Q_\mathrm{rms} \le 28\,\mu\mathrm{K}$ for a 95% confidence interval [17]. The uncertainty here includes both statistical errors and systematic errors, which are dominated by the effects of galactic emission modeling. This level of quadrupole anisotropy allows one to set general limits on anisotropic expansion, shear, and vorticity; all such dimensionless quantities are constrained to be less than about 10^{-5} [18].

For specific homogeneous cosmologies, fits to the whole anisotropy pattern allow stringent limits to be placed on, for example, the global rotation at the level of about 10^{-7} of the expansion rate [19].

22.3.3. ***The anisotropy power spectrum—theory***: The COBE-discovered [20] higher-order ($\ell > 2$) anisotropy is interpreted as the manifestation of perturbations in the energy density of the early Universe, primarily at the epoch of the CMB's last scattering. The detection of these anisotropies at just the right level for gravity to have grown all of the structure observed in today's Universe demonstrates that gravitational instability acting on primordial density perturbations was the main mechanism for structure formation.

Since theoretical models generally lead to primordial perturbations and thus $a_{\ell m}$ that are Gaussian random fields, the power spectrum in ℓ is sufficient to characterize the model. Departures from Gaussianity are certainly expected from higher order effects, but in all models the power spectrum contains the bulk of the statistical content in CMB

maps. A statistically isotropic sky means that all m's are equivalent and the power at each ℓ can be written as $(2\ell+1)C_\ell/(4\pi)$, where $C_\ell \equiv \langle |a_{\ell m}|^2 \rangle$. For an idealized full-sky observation, the variance of each measured C_ℓ is $[2/(2\ell+1)]C_\ell^2$. This sampling variance (known as cosmic variance) comes about because each C_ℓ is chi-squared distributed with $(2\ell+1)$ degrees of freedom for our observable volume of the Universe [21].

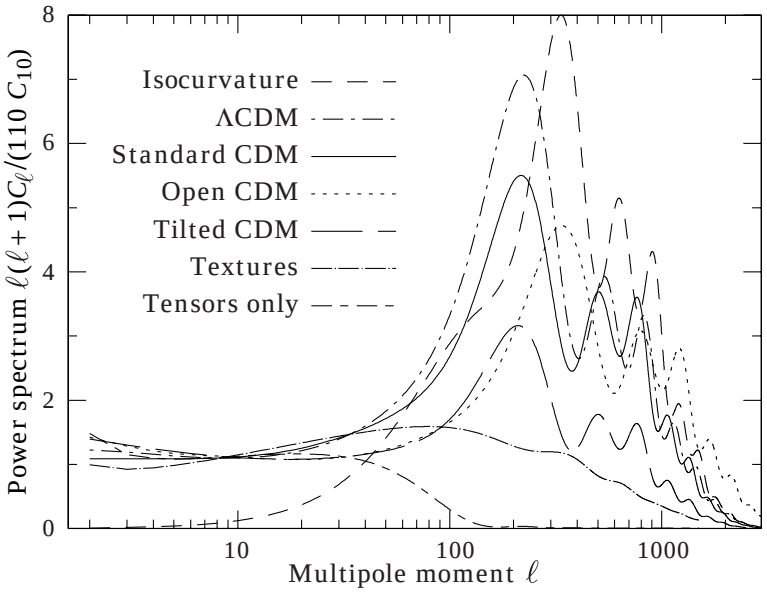

Figure 22.5: Theoretically predicted CMB anisotropy power spectra [22] in terms of $\ell(\ell+1)C_\ell$ for a range of models. The top curve is an isocurvature CDM model which has a characteristically different shape than the adiabatic models. The next four are variants of adiabatic Cold Dark Matter models. The textures model [23] is an example with perturbations seeded by topological defects. We also show a power spectrum from gravity waves (tensors), which could contribute at large angles. All the models have been normalized at $\ell = 10$ except for the isocurvature case, which was arbitrarily normalized to the height of the box. Such curves depend in detail on the precise values of the cosmological parameters, and those shown here are examples only.

Figure 22.5 shows the theoretically predicted anisotropy power spectrum for a sample of models, plotted as $\ell(\ell+1)C_\ell$ versus ℓ which is the power per logarithmic interval in ℓ or, equivalently, the two-dimensional power spectrum. If the initial power spectrum of perturbations is the result of quantum mechanical fluctuations produced and amplified during inflation, then for simple models the shape of the anisotropy spectrum is coupled to the ratio of contributions from density (scalar) and gravitational wave (tensor) perturbations [24]. In such models the large angle contribution from tensors is constrained to be $\lesssim 0.5$ [25]. However, there are other inflationary models which allow higher tensor contribution. In particular if the energy scale of inflation at the appropriate epoch is

$\simeq 10^{16}$GeV, then detection of the effect of gravitons is likely and partial reconstruction of the inflaton potential may be feasible. However, if the inflationary energy scale is $\lesssim 10^{14}$GeV, then typically density fluctuations dominate and less constraint is possible.

On angular scales corresponding to $\ell \gtrsim 50$ scalar modes certainly dominate. In the standard scenario the last scattering epoch happens at a redshift of approximately 1100 [26]. The optical thickness of the cosmic photosphere is roughly $\Delta z \sim 100$ corresponding to about 5 arcminutes on the sky, so that features smaller than this size are damped.

Anisotropies have been observed on angular scales above this damping scale by COBE and many other experiments. The initial spectrum of density perturbations is reflected in the largest angle (small ℓ) power spectrum, and for an initially scale-invariant (also referred to as 'flat') power spectrum of potential and thus metric fluctuations the prediction is that $\ell(\ell+1)C_\ell$ is approximately constant. However, perturbations can evolve significantly in the epoch $z \gtrsim 1100$ for causally connected regions, corresponding to angles $\lesssim 1^\circ\ \Omega_{\rm tot}^{1/2}$. The primary mode of evolution is through acoustic oscillations, leading to a series of peaks at small angular scales, which encode information about the primordial perturbations, geometry, matter and radiation content, and ionization history of the Universe [27]. Thus, precise measurement of the shape of the anisotropy power spectrum provides information on the amplitude and slope of the initial conditions, as well as Ω_0, Ω_B, Ω_Λ (cosmological constant), H_0 and other cosmological parameters.

The CMB anisotropies seen on the sky are a 'snap-shot' of the temperature perturbations at last scattering, with the amplitudes oscillating with spatial frequency rather like a set of standing waves. The phases of these oscillations depend on whether the initial density perturbations were 'adiabatic' (meaning that there was no change to the entropy per particle for each species) or 'isocurvature' (meaning that, for example, matter perturbations compensated radiation perturbations so that the total energy density remains unchanged). Within the family of adiabatic models, the location of the first acoustic peak is predicted to be at $\ell \sim 220\ \Omega_{\rm tot}^{-1/2}$ or $\theta \sim 0.6^\circ\ \Omega_{\rm tot}^{1/2}$ and its amplitude is a calculable function of the parameters (see Fig. 22.5).

22.3.4. ***The anisotropy power spectrum—data***: Mapping experiments provide anisotropy information on angular scales from the beam-size to the size of the map. However, for less than full sky coverage the ℓ modes are correlated. Hence fits to experimental data are usually quoted as a series of 'band powers', defined as $\ell(2\ell+1)C_\ell/4\pi$, which are determined by assuming constant fluctuation level over chosen bands of multipoles. Some results are reported using top-hat bands in ℓ, while others use an orthogonalization procedure, which makes the band-power errors independent, but causes the ℓ-band coverage to overlap somewhat.

It has been clear for several years that there is more power at sub-degree scales than at COBE scales [27]. More recent data have indicated that there is a well-defined, localized primary peak, with a second and further peaks starting to be detected (see Fig. 22.6).

Recent experimental results from the Boomerang 98 [28] and MAXIMA-1 [29] balloon flights and from a new generation of interferometric experiments, DASI [30] and CBI [31], have dramatically improved the power spectrum measurements. It is now clear that the spectrum as a whole possesses the series of acoustic peaks which are expected for adiabatic-type perturbations (compare Fig. 22.5 and Fig. 22.6). It is difficult to generate these features by an incoherent causal mechanism, such as with topological defects, and isocurvature models also generically give the wrong shape. Indeed the mere presence of the undulations in the power spectrum tells us both that the initial conditions were 'synchronized' over the largest observable scales, and that acoustic oscillations were an essential part of the physics of density perturbation evolution. This is conformation of a basic picture laid down at least as early as the 1970s [34].

Thus the present data appear to point to models with adiabatic and apparently acausal fluctuations. Since inflation is the only mechanism proposed to provide the large-scale homogeneity and anisotropy observed in the universe and to produce these apparently acausal fluctuations, one may consider the current CMB data as supporting the inflationary paradigm.

Within the adiabatic scenario, the position of the primary acoustic peak implies that the Universe is close to flat [35]. For Boomerang the constraint is $\Omega_{\rm tot} = 1.02 \pm 0.06$ [28], and in addition the initial conditions are constrained to have slope $n = 0.96 \pm 0.10$, and the baryon density is consistent with BBN estimates, with $\Omega_{\rm B} h^2 = 0.022 \pm 0.04$. Limits from the MAXIMA-1 [36] and DASI [37] experiments are similar. Combining the CMB data with other cosmological information (from supernovae, large-scale structure etc.) leads to tighter constraints on these and other parameters [28,38,39]. The best-fit model is close to the popular Λ-dominated CDM model. This is also consistent with independent observations indicating that the matter density $\Omega_{\rm M} \simeq 0.3$ (*e.g.* see Ref. 40), which together with the near flatness implies that there is some unknown contribution of 'dark energy,' supporting the picture presented by distant supernova studies [41]. Somewhat weaker (and more model-dependent) constraints can also be placed on other cosmological parameters, such as tensor contribution, Hubble constant and optical depth back to the reionization epoch.

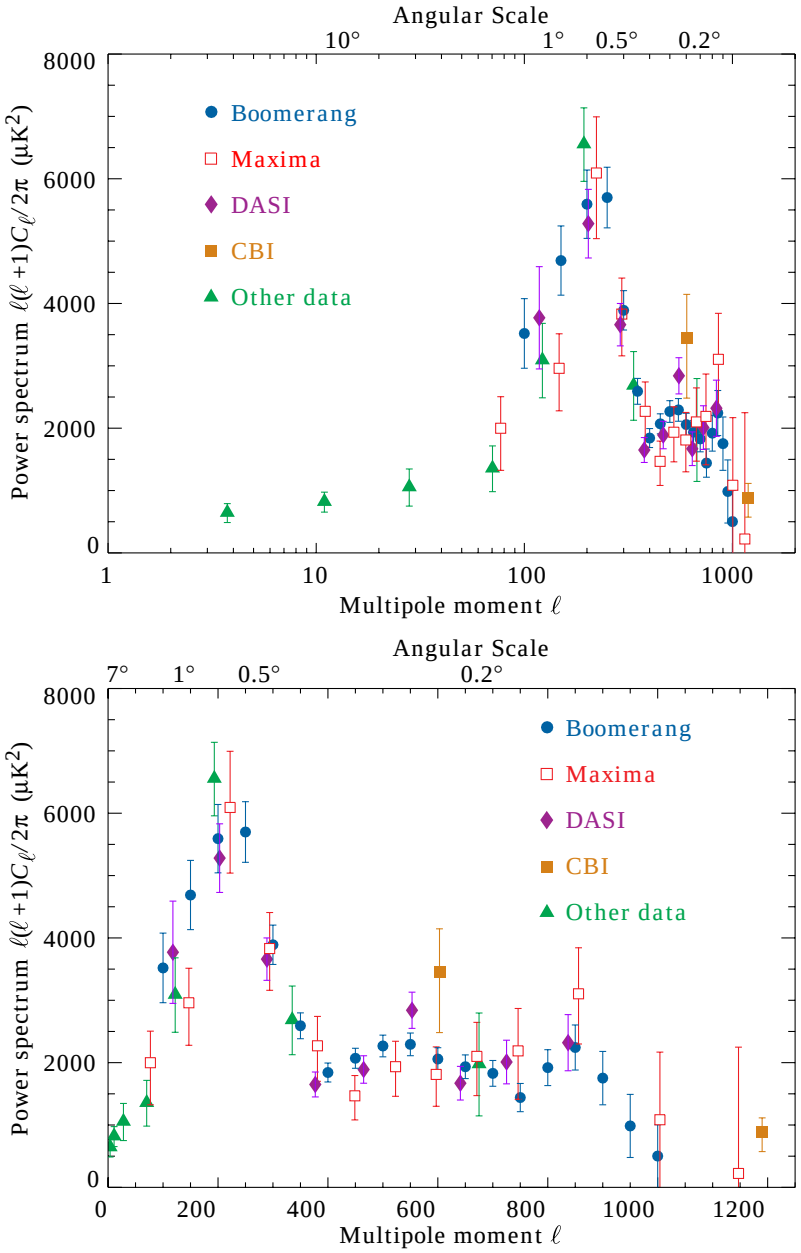

Figure 22.6: There is now so much CMB anisotropy data that it is difficult and confusing to show all the individual results. Instead the figure shows the new BOOMERANG [28] (diamonds), MAXIMA [29] (crosses), DASI [30] (triangles) and CBI [31] (squares) data, together with binned results of all previous experiments (pluses), based on data with references given in earlier versions of this Review.

Fig. 22.6 (continued): The previous data points were obtained [32] by maximizing the likelihood for a power spectrum assumed to be piece-wise constant between $\ell = 2$ and 1000, permitting experimental errors to be asymmetric, and allowing for correlated calibration uncertainties for each experiment [33]. Experimental values for the other experiments were obtained in a similar way, with the bins typically less than about 10% correlated. Note also that calibration and beam-size uncertainties for each experiment introduce correlated additional errors which are not included in the plotted error bars. The figure clearly shows a localized peak at $\ell \simeq 200$, and further structure consistent with a second and third peak as predicted in standard models. Some upper limits at smaller angular scales, indicating further evidence for a drop-off at high ℓ, have not been shown.

In addition it is also possible to put limits on other aspects of physics, for example the neutrino chemical potentials [42] or time variation of the fine-structure constant [43]. Further particle physics constraints will follow as the anisotropy measurements increase in precision.

New data are being acquired at an increasing rate, with a large number of improved ground- and balloon-based experiments being developed. The current suite of experiments has already mapped out the CMB anisotropy power spectrum to an accuracy which allows the determination of several parameters at the 10 % level. A vigorous sub-orbital and interferometric program should push those numbers further in the next few years. In addition the Microwave Anisotropy Probe (MAP) satellite was launched successfully in June 2001, with results expected at the end of 2002. This will be followed by the more ambitious Planck mission, scheduled for launch in 2007. The improved sensitivity, freedom from Earth-based systematics, and all-sky coverage of these satellites allow a simultaneous determination of many of the cosmological parameters to unprecedented precision: for example, $\Omega_{\rm tot}$ and n to about 1%, Ω_B and H_0 at the level of a few percent [44]. A great many additional 'higher order' effects, such as gravitational lensing, should also be detectable in the Planck data set. And just as with the frequency spectrum, precise measurement of the anisotropies should lead to additional constraints on any particle physics effects which operate at $z \sim 1000$ or over the largest accessible scales [45].

22.3.5. ***Polarization anisotropies***: Since Thomson scattering of the anisotropic radiation field also generates linear polarization at the roughly 5% level [46] of its anisotropy amplitude, there is additional cosmological information to be gleaned from polarization measurements. Although difficult to detect, the polarization signal should act as a strong confirmation of the general paradigm. Furthermore, detailed measurement of the polarization signal provides more precise information on the physical parameters. In particular it allows a clear distinction of any gravity wave contribution, which is crucial to probing the $\sim 10^{16}$ GeV energy range. The best current polarization limits are at the roughly 10μK level from the POLAR experiment [47] at large angular scales and the PIQUE experiment [48] at smaller scales. Other experiments currently underway are expected to reach sensitivity levels which can detect the polarization anisotropies and begin to map out their power spectrum and cross-correlation with the anisotropy.

However, the fulfillment of the promise of constraining any gravity wave signal may await an even more sensitive generation of satellites.

References:

1. R.A. Alpher and R.C. Herman, Physics Today **41**, No. 8, p. 24 (1988).
2. A.A. Penzias and R. Wilson, Astrophys. J. **142**, 419 (1965);
   R.H. Dicke *et al.*, Astrophys. J. **142**, 414 (1965).
3. K.C. Roth and J.M. Bauer, Astrophys. J. **515**, L57 (1999);
   R. Srianand, P. Petitjean, and C. Ledoux, Nature **408**, 931 (2000).
4. P.J.E. Peebles, "Principles of Physical Cosmology," Princeton U. Press, p. 168 (1993).
5. R.A. Sunyaev and Ya.B. Zel'dovich, Ann. Rev. Astron. Astrophys. **18**, 537 (1980).
6. M. Birkinshaw, Phys. Rep. **310**, 98 (1999).
7. A.C. da Silva *et al.*, Monthly Not. Royal Astron. Soc. **317**, 37 (2000).
8. L. Danese and G.F. De Zotti, Astron. & Astrophys. **107**, 39 (1982);
   G. De Zotti, Prog. in Part. Nucl. Phys. **17**, 117 (1987).
9. J.G. Bartlett and A. Stebbins, Astrophys. J. **371**, 8 (1991).
10. J.C. Mather *et al.*, Astrophys. J. **512**, 511 (1999).
11. C. Burigana, L. Danese, and G.F. De Zotti, Astron. & Astrophys. **246**, 49 (1991);
    W. Hu and J. Silk, Phys. Rev. Lett. **70**, 2661 (1993);
    E.L. Wright *et al.*, Astrophys. J. **420**, 450 (1994).
12. D.J. Fixsen *et al.*, Astrophys. J. **473**, 576 (1996).
13. J.C. Mather *et al.*, Astrophys. J. **420**, 439 (1994).
14. M. Bersanelli *et al.*, Astrophys. J. **424**, 517 (1994).
15. S. Courteau *et al.*, Astrophys. J. **544**, 636 (2000).
16. A. Kogut *et al.*, Astrophys. J. **419**, 1 (1993);
    C. Lineweaver *et al.*, Astrophys. J. **470**, L28 (1996).
17. C.L. Bennett *et al.*, Astrophys. J. **464**, L1 (1996).
18. W.R. Stoeger, M.E. Araujo, and T. Gebbie, Astrophys. J. **476**, 435 (1997); erratum **522**, 559 (1999).
19. A. Kogut, G. Hinshaw, and A.J. Banday, Phys. Rev. **D55**, 1901 (1997);
    E.F. Bunn, P. Ferreira, and J. Silk, Phys. Rev. Lett. **77**, 2883 (1996).
20. G.F. Smoot *et al.*, Astrophys. J. **396**, L1 (1992).
21. M. White, D. Scott, and J. Silk, Ann. Rev. Astron. & Astrophys. **32**, 329 (1994).
22. U. Seljak and M. Zaldarriaga, Astrophys. J. **469**, 437 (1996).
23. U.-L. Pen, U. Seljak, and N. Turok, Phys. Rev. Lett. **79**, 1611 (1997).
24. D.H. Lyth and A. Riotto, Phys. Rep. **314**, 1 (1999).
25. J.P. Zibin, D. Scott, and M. White, Phys. Rev. D 60,123513(1999).

26. S. Seager, D.D. Sasselov, and D. Dcott, Astrophys. J. Supp. **128**, 407 (2000).
27. D. Scott, J. Silk, and M. White, Science **268**, 829 (1995);
W. Hu, J. Silk, and N. Sugiyama, Nature **386**, 37 (1996).
28. C.B. Netterfield *et al.*, Astrophys. J., in press, `astro-ph/0104460`.
29. A.T. Lee *et al.*, Astrophys. J. **561**, L1 (2001).
30. N.W. Halverson *et al.*, Astrophys. J., in press, `astro-ph/0104489`.
31. S. Padin *et al.*, Astrophys. J. **549**, L1 (2001).
32. E. Pierpaoli, D. Scott, and M. White, Science, **287**, 2171 (2000).
33. J. R. Bond, A.H. Jaffe, and L.E. Knox, Astrophys. J. **533**, 19 (2000).
34. P.J.E. Peebles and J.T. Yu, Astrophys. J. **162**, 815 (1970);
Doroshkevich, Ya.B. Zel'dovich, and R.A. Sunyaev, Sov. Astron. **22**, 523 (1978).
35. S. Dodelson and L. Knox, Phys. Rev. Lett. **84**, 3523 (2000);
A. Melchiorri *et al.*, Astrophys. J. **536**, L63 (2000);
M. Tegmark and M. Zaldarriaga, Astrophys. J. **544**, 30 (2000).
36. R. Stompor *et al.*, Astrophys. J. **561**, L7 (2001).
37. C. Pryke *et al.*, Astrophys. J. **568**, 26 (2002).
38. X. Wang, M. Tegmark, M. Zaldarriaga, PRD, in press, `astro-ph/0105091`.
39. P. de Bernardis *et al.*, Astrophyscal Journal, in press, `astro-ph/0105296`.
40. R.G. Carlberg *et al.*, Astrophys. J. **462**, 32 (1996);
P. Coles and G.F.R. Ellis, "Is the Universe Open or Closed?", Cambridge University Press, Cambridge (1997).
41. S. Perlmutter *et al.*, Astrophys. J. **517**, 565 (1999);
A.G. Riess *et al.*, Astron. J. **116**, 1009 (1998).
42. S.H. Hansen *et al.*, Phys. Rev. **D65**, 023511 (2002).
43. P.P. Avelino *et al.*, Phys. Rev. **D64**, 103505 (2001).
44. M. Tegmark *et al.*, Astrophys. J. **530**, 133 (2000);
S. Prunet, S.K. Sethi, and F.R. Bouchet, Monthly Not. Royal Astron. Soc. **314**, 348 (2000).
45. M. Kamionkowski and A. Kosowsky, Ann. Rev. Nucl. Part. Sci. **49**, 77 (1999).
46. W. Hu and M. White, New Astron. **2**, 323 (1997).
47. B.G. Keating *et al.*, Astrophysical Journal, in press, `astro-ph/0107013`.
48. M.M. Hedman *et al.*, Astrophys. J. **548**, L111 (2001).

CMB Spectrum References:

1. **FIRAS:** J.C. Mather *et al.*, Astrophys. J. **420**, 439 (1994);
D. Fixsen *et al.*, Astrophys. J. **420**, 445 (1994);
D. Fixsen *et al.*, Astrophys. J. **473**, 576 (1996);
J.C. Mather *et al.*, Astrophys. J. **512**, 511 (1999).

2. **DMR:** A. Kogut *et al.*, Astrophys. J. **419**, 1 (1993);
A. Kogut *et al.*, Astrophys. J. **460**, 1 (1996).
3. **UBC:** H.P. Gush, M. Halpern, and E.H. Wishnow, Phys. Rev. Lett. **65**, 537 (1990).
4. **LBL-Italy:** G.F. Smoot *et al.*, Phys. Rev. Lett. **51**, 1099 (1983);
M. Bensadoun *et al.*, Astrophys. J. **409**, 1 (1993);
M. Bersanelli *et al.*, Astrophys. J. **424**, 517 (1994);
M. Bersanelli *et al.*, Astrophys. Lett. and Comm. **32**, 7 (1995);
G. De Amici *et al.*, Astrophys. J. **381**, 341 (1991);
A. Kogut *et al.*, Astrophys. J. **335**, 102 (1990);
N. Mandolesi *et al.*, Astrophys. J. **310**, 561 (1986);
G. Sironi, G. Bonelli, & M. Limon, Astrophys. J. **378**, 550 (1991).
5. **Princeton:** S. Staggs *et al.*, Astrophys. J. **458**, 407 (1995);
S. Staggs *et al.*, Astrophys. J. **473**, L1 (1996);
D.G. Johnson and D.T. Wilkinson, Astrophys. J. **313**, L1 (1987).
6. **Cyanogen:** K.C. Roth, D.M. Meyer, and I. Hawkins, Astrophys. J. **413**, L67 (1993);
K.C. Roth and D.M. Meyer, Astrophys. J. **441**, 129 (1995);
E. Palazzi *et al.*, Astrophys. J. **357**, 14 (1990).
7. **GMRT:** A. Raghunathan and R. Subrahmanyan, J. Astron. Astrophys. **21**, 1 (2000).